Chapter 3

Synthesis of Chemical Elements and Solid Structures in Atomic-Nuclear Reactions in Dense Gas-Metal Systems Irradiated by γ Rays

Roland Wiśniewski

Additional information is available at the end of the chapter

http://dx.doi.org/10.5772/intechopen.78740

Abstract

The new effects observed in dense gas-metals systems (example D_2-Pd) being irradiated by braking gamma quanta with threshold energy a little bellow 10 MeV, for energy about 25 MeV (giant dipole nuclear resonance—GDNR) and effects of irradiation of pure gazes (D_2, He… 10 MeV) is presented in this chapter. The irradiation time in all cases was as large as 10^5 s under large gamma flux intensity conditions (generated by electron current in used accelerators of about 20 μA). Realization of experiments were as follow: chosen gas in room temperature was compressed to high pressure (1–3 kbar) in beryllium bronze pressure chamber or in stainless steel high pressure capillary with chosen metal samples inside of it or without samples. In all cases new elements were detected in relatively large amounts, some of them are light elements, i.e., C, O and the others are heavy elements, i.e., Pb, Bi. At GDNR with Pd, V and other metals, unexpected phenomena as shape changes, "micro-protuberances," micro objects of specific element contents, cracks of specimen surfaces were observed too. The identification of the mechanism that induced these effects is a problematic issue, trans-nuclear molecule and multinuclear reaction concepts could be used to explain these induced effects. The justification of carbon generation in the samples is shortly described.

Keywords: gamma quanta irradiation, dense gas-metal systems, fission, fusion reaction, transmolecule, chemical composition

1. Introduction and historical outline

In the 2005, Didyk [1] from the Join Institute for Nuclear Research in Dubna (RF) was visited the National Centre for Nuclear Research (Otwock-Świerk, Poland). He was introduced to

high pressure method for hydrides synthesis [2] by Author, and close cooperation between them was born. In their first experiment they have placed the Pd samples into the gaseous deuterium in increased pressure (3–5 kbar), and exposed this setup to gamma radiation, in order to significantly increase the content of deuterium in palladium (D/Pd > 1) by deuterium atomization and the call to other possible phenomena accompanying referred to the radiation. The electron accelerator Microtron MT-25 in the Flerov Laboratory of Nuclear Reactions JINR in Dubna, was used as the gamma radiation source. Intense braking radiation (using tungsten target, thickness 2.5 mm) with electron current 10–24 μA), long exposure times (E5s) was applied to the setup resulted in the transformation which one of the effects was creation in macro-scale objects (element composition). After this, unexpected results, experiments were continued. The range of threshold energy of gamma-quantum in the greater part of them was around 10 MeV, in a few cases, was increased up to 24 MeV. The latter value corresponds to the scope of the giant nuclear dipole resonance of exposed samples. Initially, the high-pressure chamber material were seen only as the normal processes of absorption of gamma radiation, provided through a special item of apparatus-cork related pane. Researchers conducted on pure gases (no samples in the high-pressure chamber) appeared to be surprising enough to force change of approach to explaining the results. We started to perceive results as the effect of exposure to quanta gamma the selected gases under high pressure, surrounded by metallic shell in the form of a metallic chamber with or without an object located around the centre of shell (see **Figure 1**). This idea was implemented in the form of custom designed high-pressure systems (laboratory), presented in the body of the chapter. The experience described below, you need to request the presence of a number of nuclear processes (fission and fusion) initiated by photo reactions (gamma rays) and certain more or less complicated physical and chemical processes. Effects, in the sense of the masses of generated objects (and their composition) are macroscopic, which allows to talk about the possibility of new nuclear technology (engineering) allowing to produce heavy elements such, as rare earth elements. Work related to the construction of high-pressure apparatus, developing of different measurements systems, gas filling under high pressure, preparation of samples, formal documentations took place at Pressure Investigation Laboratory of the National Centre for Nuclear Research in Poland. The high-pressure equipment was built by Author and PhD. Wilczyńska-Kitowska T. Irradiation procedures were carried out in the Joint Institute for Nuclear Research in Dubna, in the Flerov

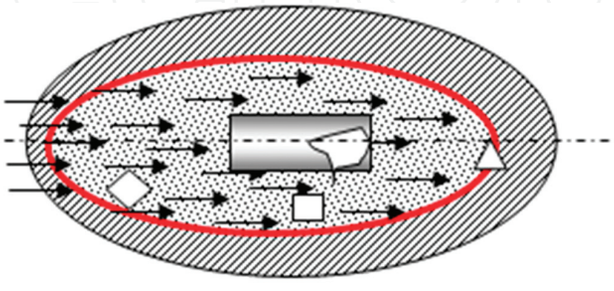

Figure 1. Simplified model of conducted experiments. The arrows presents high energy gamma quanta stream passing through the inlet port of the pressure shell. Polygon character symbolizes the central object changes. Square character symbolizes objects which were observed inside of the chamber and triangular character changes in inner element (red line) separates the gas from the pressure shell.

http://dx.doi.org/10.5772/intechopen.78740

Laboratory of Nuclear Reactions. Investigation of obtained objects, using scanning electron microscopy (SEM) and X-ray micro sound analyzer (XRMPA) were performed in the Analytical Centre of the Skobeltsyn Laboratory of Lomonosov Moscow State University and at the Research Institute for Perspective Materials and Technologies in Moscow. We have observed: macroscopic surface changes, the emergence of new elements in the macroscopic amount, change the shape of the samples, micro eruption from the metallic surface and exposed to weight changes of investigated samples.

In order to validate our results a number of additional experiments were conducted: (A) the main investigation element—palladium sample—was subjected to operation of pure deuterium gas at a pressure of approximately 20 kbar over a period of several months. After dismounting, no changes resembling result received after irradiation of the similar setup, in the object itself or chamber were found. The currently known classic effects (volume change, resistance, etc.) associated with the process of saturation Palladium by deuterium gas under pressure was tested by the author much earlier [3]. (B) Irradiation of the sample of palladium, without presence of high-pressure gas did not resulted in any changes on the surface of the sample (typical radiation effects such as structural defects, were not taken into account). (C) High-pressure chamber, with the sample of palladium, and average vacuum after irradiation did not show any of our research typical effects. (D) At lowered deuterium pressure up to 60 bar, irradiation time 1.3E5s, electron current 1.1E14 s^{-1} with typical Pd specimen (purity of 99.997%) no effect was observed either.

In authors opinion, farther studies of presented results and proposed interpretation, should result in new specific methodology of basic investigation, and new technology in the future. Since, known classic nuclear effects and theories (and possible physical-chemical processes) are fundamental for interpretation of observed phenomena by author and his co-operators but others new ideas are desirable. Why so relatively small pressure (1000 bar) of gases play so essential role? Does this "trigger" pressure value differs for different gases?

Simplified model of conducted experiments is shown in **Figure 1**.

The arrows presents high energy gamma stream passing through the inlet port of the pressure shell. Polygon character symbolizes the central object changes. Square character symbolizes objects which were observed inside of the chamber and triangular character changes in inner element (red line) separates the gas from the pressure shell. Similar objects can be exist in similar condition in some time in somewhere is Cosmos. What effects would took place there we can see as results of our experiments described below.

The following experimental investigations were carried out:

1. Simple system Pd-D_2, classic type of high-pressure chamber (CTHPC) [4].
2. Simple system Pd-D_2, (CTHPC), Pd-D [5].
3. Simple system Pd-H_2, (CTHPC) [6].
4. Double system Pd-Re-D_2, finger type HPC, giant dipole nuclear resonance (GDNR) [7].
5. Double system, Al-YMn2-D_2, FTHPC, GDNR [8].

6. Double system, V-SS-D_2, CTHPC, GDNR [9].
7. Complex system, Al-YMn2-Al-YMn2-Cu-SS-D2, FTHPC, GDNR [10].
8. Complex system, Sn-Mo-Fe-Ni-Bi-Ta-Cu-H_2, CTHPC [11].
9. Pure Helium, CTHPC [12–14].
10. Pure Hydrogen, CTHPC [15].
11. Pure Deuterium, CTHPC [16].

In this chapter, as examples of gamma irradiation investigations in metal-dense gases systems: Pd-D_2 (10 MeV), Pd-Re-D_2 (24 MeV) and pure H_2, D_2 and He (10 MeV) are presented.

2. Experimental setup

A hydrogen (deuterium) high-pressure chamber (H(D)HPC) has been designed. The first high-pressure apparatus for gaseous hydrogen (deuterium) was constructed and build by Author [3]. Presented here, two types, apparatus are portable and adapted to γ irradiation. The scheme of the DHPC with deuterium and Pd specimen inside, used by us in first experiments, is presented in **Figure 2**. Inside the DHPC with an inner cylinder of diameter of 0.4 cm there was placed a cylindrical Pd-rod (with 99.98% purity) of diameter 0.38 cm and length 0.5 cm. A distance manganin sleeve of length 0.6 cm was disposed between the Pd-rod and brass screw of length 0.5 cm and diameter 0.4 cm. The DHPC inside volume was equal to $V_D = 0.264$ cm^3 and filled with molecular deuterium under the pressure of about 3 kbar. At such pressure the molecular deuterium density was about $n_{D_2} = 2.593 \times 10^{22}$ mol.D_2/cm^3 (see [26]). Therefore, the overall number of deuterium atoms in the DHPC inner volume was about ND = 1.4×10^{22} at. D. In **Figure 3** a last form of this apparatus is presented. Main changes concern to elimination of any plastic type O-ring system and create full CuBe brass environment of investigated metal-gas system.

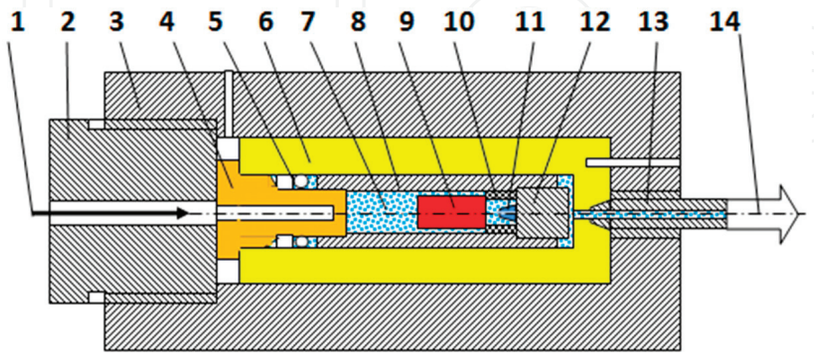

Figure 2. The schematic drawing of high-pressure apparatus (DHPC). 1—γ-quanta, 2—closing screw with hole, 3—reinforcing high-pressure chamber body, 4—$Cu_{0.98}Be_{0.02}$ "window" plug, 5—high-pressure seals, 6—$CuBe_2$ high-pressure chamber, 7—(hydrogen) deuterium under high pressure, 8—brass sleeve, 9—investigated Pd-rod, 10—distance manganin sleeve, 11—expected reaction product, 12—brass screw, 13—high-pressure-connecting capillary, 14—high-pressure valve, strain gauge pressure sensor and gas filling inlet [4].

http://dx.doi.org/10.5772/intechopen.78740

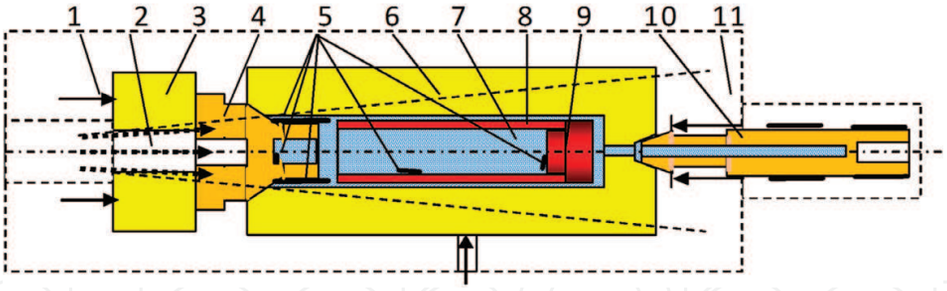

Figure 3. Elements of modified high-pressure apparatus exposed to irradiation by gamma rays: 1—Pressure for sealing of the closing screw to the window plug, 2—Gamma ray flux of initial diameter of 5 mm, 3—$CuBe_2$ element inserted in the closing screw, 4—Gamma ray window-plug, 5—surface regions where carbon foils and other particles were observed in large quantities, 6—high-pressure chamber reinforced by outer element, 7—gas (under pressure), 8—pure copper (or $CuBe_2$) sleeve, 9—pure copper (or $CuBe_2$) closing element, 10—gas supplying and pressure measurement strain gauge device, 11—schematically shown reinforcing outer element.

Figure 4 shows part of this DHPC adapted for irradiation by γ-quanta of sets of specimens from various materials in the shape of wires with relatively small diameters. For this apparatus the walls were made of 204 stainless steel (204SS) to exclude such chemical elements, observed in the first experiment, as copper and zinc. These elements comprised the degraded layer of thickness over 80 μm in palladium as in the first experiment [4].

Two type experiments to study γ-quanta irradiation effects were carried out at the electron accelerator MT-25, FLNR, JINR using two electron beams of energies 9.3 and 25 MeV, which correspond to γ-quanta energy < 8.8 and 23 MeV, respectively. The electron current at the tungsten convector shaped as a disk of 40 mm diameter and 2.5 mm thickness used to transform the electron flux into gamma rays was (1–1.5) $\times$ 10^{14} electron/s. It can be supposed that generated gamma flux is the same of order. The electron beam was 6–7 mm in diameter. The beam spread of gamma quanta at the intensity half-height amounted to $10 \pm 1^{\circ}$ in horizontal and $8 \pm 1^{\circ}$ in vertical direction. Right behind the convector, an electron absorber of 25 mm thickness made from D16T duralumin was placed.

The γ-quanta spectra Nγ(Eγ) were calculated using the expressions presented in [17].

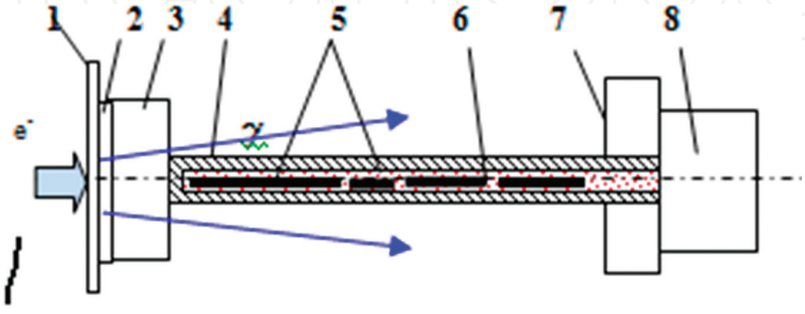

Figure 4. A scheme of capillary type DHPC intended for irradiation of materials: 1—vacuum system wall, 2—tungsten target, 3—alumina absorber, 4—capillary type pressure chamber, 5—specimens: One Pd and three of different length Re, 6—gaseous deuterium, 7—safety wall, 8—gas fill up, pressure and temperature measurement systems.

Calculation of the energy spectrum of γ-quanta from the units of measurement in MeV^{-1}·$steradian^{-1}$ into the flux density of γ-quanta in cm^{-2} and per area of the input window plug at the DHPC-target gave value about 3%. We can now calculate [18], for energy intervals ΔE_γ = 1 MeV, the number of neutrons and protons produced by γ-quanta in the photofission reaction D(γ,n)p—mostly expected in case of irradiated D_2—with the maximal energies $E_\gamma^{max} = 8.8$ MeV and $E_\gamma^{max} \leq 23.0$ MeV using the expression:

$$Y(E_\gamma^{max}) = \beta \cdot N_D \cdot \int_{\Delta W}^{E_\gamma^{max}} \sigma_{D(\gamma,nlp)}(E_\gamma) \cdot N_\gamma(E_\gamma) dE_\gamma \quad (1)$$

where ΔW = 2.22 MeV is the deuteron bond energy. In [4] adequate cross sections, histograms with neutron and proton yields $N_n(E_\gamma)$ and $N_p(E_\gamma)$, respectively, at two ranges $n_H \approx 8.8$ Mev and $p_H \approx 23$ Mev are presented for two energies of electron beams of 1 μA.

Developed measurement of pressure technique (pressure sensor, with strain gauge elements shown in **Figure 3**) was used in our condition continuously and with sufficient high accuracy. Temperature measurements were realized using standard thermoelement equipment. Irradiations processes performed in our experiments were fully controlled by Laboratory Security Service as normal procedure in such type experiments.

3. Induced effects in gas (D2) and metal-gas systems (Pd-D2)

Here is presented information based on the first experiment [4], i.e., on irradiation process of Pd-D_2 system under pressure of gaseous deuterium about 3 kbar. During the whole time of DHPC exposure to γ-quanta t ≈ 2.22 × 10^4 s, the average current of the electron beam was ≈ 7 μA. The total number of neutrons and protons produced by γ-quanta per experiment $N_{n,p}$ = 3.23 × 10^{10} n, p. During the irradiation by γ-quanta the DHPC was cooled by a flux of compressed air at the temperature ≈ 20°C, nevertheless, the temperature of the DHPC external surface significantly exceeded 100°C.

Prior to opening of the DHPC, some hold-up time aimed to decrease induced activity was allowed to elapse before the chamber was finally opened. The Pd-rod with the external initial diameter 3.8 mm was found to be wedged due to its increased overall dimensions inside the brass sleeve with the inside diameter d = 4 mm. After 3 days the palladium specimen decreased in size and was easily extracted. Relative diameter change ((0.2/4)100% = 5%) was caused by other than the normal volume change related to beta phase appearance in PdD system.

3.1. Synthesized novel object (SNO)

On the flat inside surface of the brass screw (see **Figure 2**, p. 12), there was discovered a synthesized novel object (SNO). The optical (a) and SEM (b) scanning electron microscopy images of this object are presented in **Figure 5**. Because of high value of dielectric permeability, the surfaces of the SNO object and brass screw were covered with a thin gold layer of thickness up to 1000 Å (see **Figure 5b**).

http://dx.doi.org/10.5772/intechopen.78740

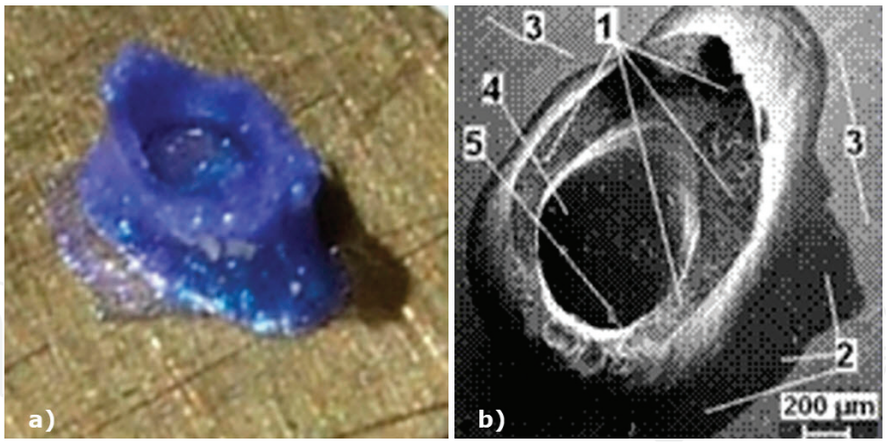

Figure 5. A view photo of the brass screw with the synthesized novel object (SNO, informal name Annavit [12]) (a) and "volcano" image with the SNO made by scanning electron microscopy (b) [4].

Let us present concentrations of chemical elements (at.%) obtained by microelement analysis from the surface brass around the SNO object ($3_{1,2,3,4,}$ **Figure 5b**). They are as follows (characteristic data): C^6 - 39.70, O^8 - 0.86, Fe^{26} - 0.25, Cu^{29} - 29.29, Zn^{30} - 18.40, Nb^{41} - 1.49. Concentrations of chemical elements (at.%) gained by microelement analysis from the surface in the spread melt "lava" near the SNO ($2_{1,2,3,}$ **Figure 5b**) are as follows: (characteristic data): C^6 - 55.01, 0^8 - 35.08, Mg^{12} - 1.48, Al^{13} - 0.92, Si - 2.26, K^{19} - 0.35, Ti^{22} - 2.47, Cu^{29} - 0.85, Zn^{30} - 0.49, Au^{79} - 1.10.

The element composition (wt.%) on the top of SNO object for four measured points ($1_{,1234}$ **Figure 5b**) is as follows:

1.1: C^6 - 26.81, 0^8 - 37.78, Mg^{12} - 0.44, Al^{13} - 5.27, Si^{14} - 6.88, K^{19} - 1.7, Ca^{20} - 0.31, *Ti^{22} - 13.17*, Fe^{26} - 0.31, Cu^{29} - 1.17, Zn^{30} - 0.67, Au^{79} - 5.49;

1.2: C^6 - 50.5, 0^8 - 38.43, Mg^{12} - 1.62, Si^{14} - 2.92, Ti^{22} - 0.32, Zn^{30} - 0.81, Au^{79} - 5.39;

1.3: C^6 - 38.51, 0^8 - 26.35, Mg^{12} - 0.74, Al^{13} - 4.81, Si^{14} - 7.36, Cl^{17} - 0.27, K^{19} - 1.76, *Ti^{22} - 9.73*, Cu^{29} - 0.7%, Zn^{30} - 0.83, Au^{79} - 8.93;

1.4: C^6 - 56.69, 0^8 - 30.39, Mg^{12} - 1.7, Al^{13} - 0.89, Si^{14} - 4.03, K^{19} - 0.28, Ti^{22} - 2.54, Zn^{30} - 0.67, Au^{79} - 2.81.

As one can see, at two measured points the high concentration of Ti (13.17 and 9.73 wt.%) is accompanied by inclusion of associated elements as Al (5.27 and 4.81 wt.%), Si (6.88 and 7.36 wt.%) and K (1.7 and 1.76 wt.%), and also such elements as Fe, Ca, Cl and Mg.

All the elements observed on the flat top of the "volcano with a crater at the center" object were present on the molten patch or the so-called "lava," although in changed quantities are as follows: Ti—4.44 wt.%, Al—1.04 wt.%, Si—2.65 wt.%, Mg—1.77 wt.% and higher concentrations of Cu and Zn which form the basis of the brass screw, i.e., Cu—2.26 wt.%, Zn—1.32 wt.%. This can be explained by that the spread layer is thin and the electron beam partially reaches the brass substrate during the analysis.

Some various objects such as re-crystallized and melted pieces of brass, as flat thin plates with various forms and small pieces of Pd particles were observed at the bottom of crater (point 4,

Figure 5b). It is necessary to note that all these objects are weakly bond with the floor of crater again with flat object.

The element composition (at.%) of one planar plate-like objects (p. 5 **Figure 5b**), located on the "crater" floor, is as follows: C^{6} - 19.57, 0^{8} - 20.29, K^{19} - 3.98, Ti^{22} - 50.65 at.% (main elements). The "crater" floor itself has the same chemical composition as these isolated, floor-covering plate-like objects.

On the crater floor one observes the smaller sphere-like objects also complex objects and multiple plate-like objects of size 5–10 μm. The plate-like objects comprise large quantities of Ti—66.42 ± 0.97 wt.% contained as rutile (TiO_2), as was shown by X-ray analysis. It should be noted that on the measured patches of the crater top there was observed a substantial amount of K—4.26 ± 0.16 wt.%, which is close in nucleus charge to titanium, and Fe—1.17 ± 0.07 wt.%, as well as small quantities of Cu—3.68 ± 0.12 wt.% and Zn—2.54 ± 0.10 wt.%. The copper and zinc concentrations in the plate-like objects can be compared to their concentrations on top of the SNO crater walls and in the alloy on the brass screw surface.

The element composition (at%) of the analyzed surface of another complex recrystallized object form on the floor of crater (p. 4, **Figure 5b**) is as follows: C^{6} - 20.87, 0^{8} - 8.80, Al^{13} - 3.31, Ti^{22} - 2.76, Fe^{26} - 1.35, Cu^{29} - 35.56, Zn^{30} - 21.36, Au^{79} - 2.85.

Then the more detail repeated measurements of brass surface with SNO (**Figure 2** p. 11) were made along the brass screw (**Figure 1** p. 12) diameter for check of obtained results using another electron microscope with X-ray analysis.

Screw surface containing congealed "lava from the crater" together with the chemical composition measured at six points from the right edge of the brass screw towards the melt were measured too [4].

3.2. Surface objects and element composition of Pd specimen

The surface studies of both Pd rod edges and side were carried out before (left positions) and after irradiation (right positions) is presented in **Figure 6**. The deformed Pd sample and the fantastic surface object of the irradiated Pd-rod edge which was close to SNO was obseved.

The element analysis (wt.%) of the Pd-rod edge with seven measured points (**Figure 7**, left and right spectra) is as follows:

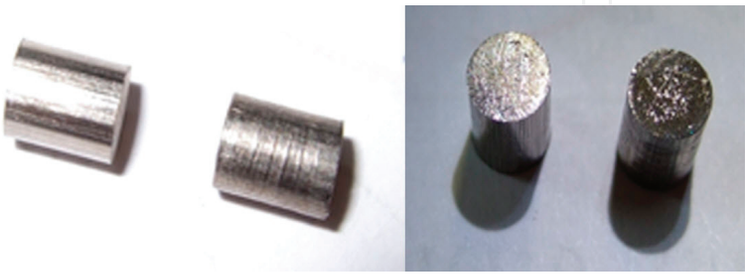

Figure 6. Pd-rod specimen before and after irradiation (one can see it layered structure) and black surface view, which was close to SNO.

http://dx.doi.org/10.5772/intechopen.78740

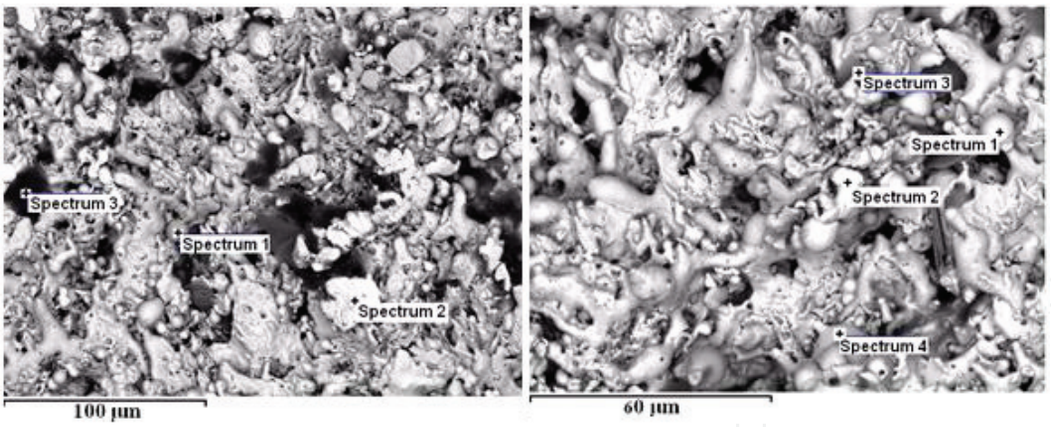

Figure 7. SEM image of the irradiated by γ-quanta edge of the Pd-rod close to SNO [4].

Ll: 0^{8} - 3.05, Cu^{29} – 49.25, Zn^{30} - 37.99, Pd^{46} - 1.51,

L2: Cu^{29} - 12.55, Zn^{30} - 5.92, Pd^{46} - 74.26,

L3: 0^{8} - 14.64, Si^{14} - 0.65, S^{16} - 1.08, Ca^{20} - 0.71, Ti^{22} - 1.38, Cu^{29} - 8.29, Zn^{30} - 3.81, Pd^{46} - 25.66,

R1: Cu^{29} - 6.45, Zn^{30} - 3.02, Pd^{46} - 88.18,

R2: Cu^{29} - 3.88, Zn^{30} - 2.55, Pd^{46} - 93.58,

R3: 0^{8} - 22.76, Al^{13} - 3.37, Si^{14} - 3.4, K^{19} - 0.54, Ti^{22} - 11.61, Cu^{29} - 31.20, Zn^{30} - 10.41, Pd^{46} - 10.71,

R4: 0^{8} - 2.89, Mg^{12} - 0.38, Cu^{29} - 28.73, Zn^{30} - 7.59, Pd^{46} - 52.49.

The entire Pd-rod object turned into an inhomogeneous one, composed of separate clusters with different element compositions. That is precisely why it was impossible to remove the Pd specimen right upon opening the DHPC chamber when this specimen had significantly grown in volume. In the above case, the palladium temperature was such that it enabled processes which brought about formation in some places of copper and zinc concentrations of up to 31.20 and 10.41 wt.% (R3), 49.25 and 37.99 wt.% (L1). At the same time, the concentration of Ti was 1.38 wt.% (L3) and in some places proved to be up to 11.61 wt.% (R3) while for the associated elements it was as follows: Si—0.65 wt.%, S—1.08 wt.%, Ca—0.71 wt.% (L3), as well as for other observed elements: Al—3.37 wt.%, Si—3.4 wt.%, K—0.54 wt.% (R3).

4. Induced effects in binary metal-gas system (Pd-Re-D2)

The goal of this part of chapter is to present the peculiarities of nuclear reaction processes in two or more pure metals placed together in dense gaseous deuterium, saturated with deuterium at high pressures and then being under the action of γ-quanta with the boundary energy 23 MeV, namely, in the region of the giant nuclear dipole resonance.

Palladium specimen (99.96%, in the shape of a rod of diameter 1 mm and length 111 mm) and three rhenium specimens (99.97%, three rods of diameter 1 mm and length 13, 25 and 33 mm)

were placed in the capillary type DHPC under the pressure of gaseous deuterium of about 3.0 kbar. In this experiment irradiation by γ-quanta with the threshold energy 23 MeV was carried out during 19.5 h ($t = 7 \times 10^4$ s) at the average electron beam current (11–12)μA, $(0.5–0.7) \times 10^{14}$ s^{-1}.

Calculation of γ-quanta spectra and fluxes as well as neutron yield from the d(γ,n)p neutron photodisintegration reaction is described in detail in [4]. Intensity of gamma quanta in different points of investigated specimens is not easy to definite because of its mass absorption and space relation. For sure intensities in introduction surface of specimen and end one may differ several times.

Before opening the DHPC (**Figure 4**), the chamber pressure was measured to be 2860 bar, so definite jump down of pressure was noted. The palladium wire and three rhenium specimens placed in the chamber could be extracted only 3 days later, apparently, after deuterium desorption. The specimens, like the DHPC itself, proved to be highly activated, which did not permit X-ray microelement analysis to be performed even after a long period allowed with the aim of decreasing the induced activity: 4 months for the palladium specimens and over 8 months for the rhenium ones.

4.1. Experimental results for the palladium rod

In **Figure 8** SEM images show places of entry (a) and exit (b) of γ-quanta for the palladium rod. As it is seen, the right edge of the specimen has undergone particularly considerable changes, namely, formation of an elongated part tapering towards the end from 1 mm to 0.461 mm in diameter with a strongly changed (eroded) frontal edge about 1000 μm wide. Both at the left and right ends of the wire one can observe smaller-scale inhomogeneous in the shape of congealed blowouts from the surfaces.

Figure 9 shows congealed-solar-protuberances structures: "a"—blowout from the left surface in the direction opposite to the γ-quanta flux direction, "b"—blowout in the direction coinciding with the γ-quanta flux direction, and "c"—"pedestal" crystal structure on the surface from the direction of γ-quanta penetration. In **Table 1** there is shown element concentration at points 1–3 of observed elements on **Figure 9**. **Figure 10** provides two other interesting photos of blowouts from the end surface from the direction coinciding with the γ-quanta flux direction. In **Table 1** there is shown element concentration at points 4–5 of observed elements on **Figure 10**.

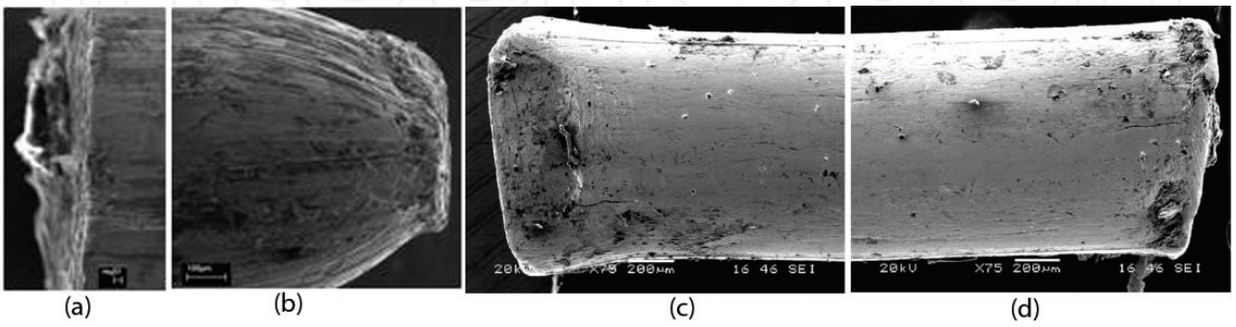

Figure 8. SEM images of the left and right ends of the Pd-rod and two sides of a Re-rod: left—place of entry of γ-quanta, right—in reverse side both specimens after irradiation at GNDR condition in D_2 gas.

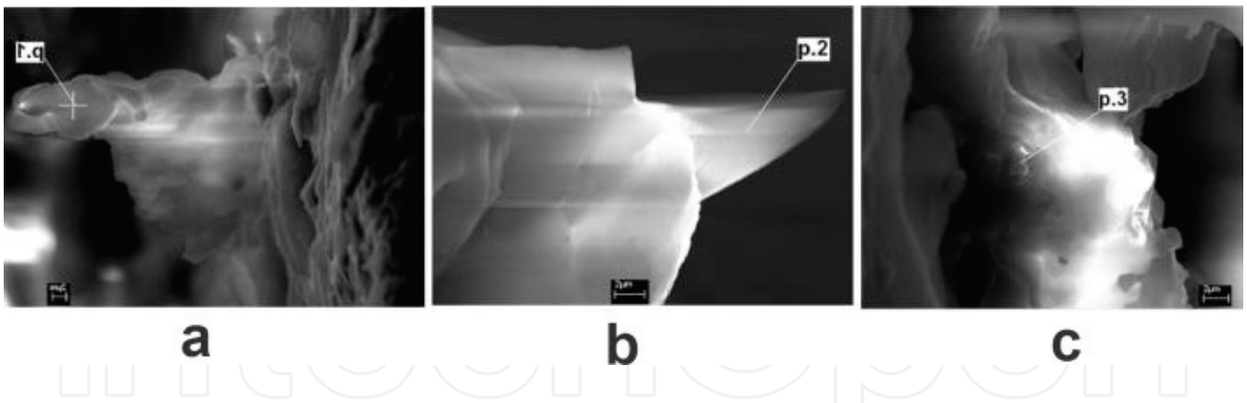

Figure 9. Congealed blowouts: from the γ-quanta entry surface (a), from second frontal surface of the palladium rod (b) and the "pedestal" of structure (c).

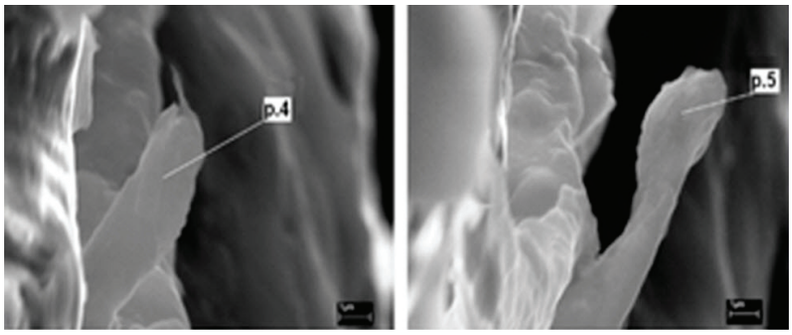

Figure 10. Two congealed blowouts on the direction of γ-quanta escape, from the right end of the palladium rod.

As is shown, the element composition of the blowouts is comprised of a series of elements which are lighter than palladium.

Figure 11 shows SEM images of two surface patches, also near the tapering part (see **Figure 8b**), with several particles on the palladium surface analyzed using XMA (**Table 2**).

Figure 12 shows SEM images of the crack and small crystals on the side surface of the palladium wire. **Table 3** shows element concentration of microcrystal and crack.

4.2. Experimental results for a rhenium rod

It should be noted first and foremost that it was possible to carry out SEM and XMA studies only by using a rhenium wire 13 mm long because it had been placed at a distance of 110 mm (behind the palladium wire) from the back wall of the DHPC entrance window, had a smaller size and, consequently, had acquired a lower induced activity. The other rhenium specimens (of the length 25 and 33 mm) were not accessible for study.

Figure 8 provides SEM images of a rhenium wire with the place of entry of γ-quanta (c) and its reverse side (d), respectively. We can compare the large deformations of both specimens Pd and Re.

Element	Point 1	Point 2	Point 3	Point 4	Point 5
	at.%	at.%	at.%	at.%	at.%
C	—	76.22	66.42	47.58	—
O	27.95	15.77	14.76	11.42	18.19
F	—	—	6.28	—	1.59
Na	—	0.53	1.16	1.02	1.85
Mg	2.68	0.26	—	38.42	58.55
Al	54.56	6.26	7.95	0.45	1.51
Si	3.28	0.07	—	0.07	0.25
S	0.95	0.05	—	0.39	0.58
Cl	0.41	0.19	0.11	0.20	0.44
K	1.42	0.16	1.46	0.13	3.86
Ca	0.52	0.03	0.24	0.10	0.43
Cr	0.54	0.08	0.15	0.12	028
Mn	0.33	0.02	—	0.28	1.06
Fe	2.37	0.34	0.75	0.01	0.44
Ni	—	0.02	—	—	0.97
Cu	1.87	0.01	—		
Zn	1.03	—	—		
Pd	0.23	—	—		
Re	1.86	—	0.74		

Table 1. Element and its concentration in blowouts shown in **Figures 9** and **10** at points 1–5.

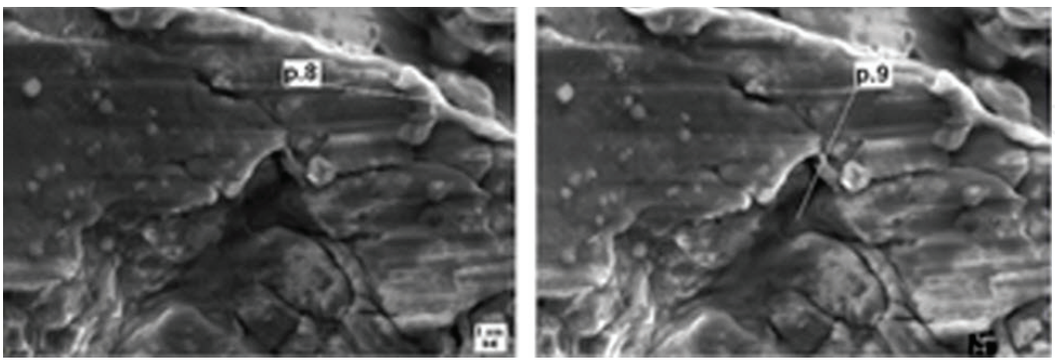

Figure 11. SEM images of a surface patch near the tapering part from **Figure 8b**.

Figure 13a shows a SEM image of surface patch of a Re crack. Once again it is of interest to estimate the concentrations of impurities produced in nuclear reactions from the most degraded cavities, i.e., from the cracks one of which is presented in **Figure 13b**. Averaged XMA analysis was carried out over three surface patches. Its results are summarized in **Table 4** (Spectra 1–4 mean points 1–4). As one can see, the entire rhenium surface is coated with a

http://dx.doi.org/10.5772/intechopen.78740

Element	Point 8	Point 9
	at.%	at.%
C	37.3	43.8
O	-	27.5
F	-	5.4
Na	-	1.0
Al	1.1	0.8
Si	-	0.4
P	-	0.3
Ca	-	0.7
Cr	0.5	-
Mn	-	0.1
Fe	0.8	0.2
Pd	60.3	17.1

Table 2. Element and its concentration in blowouts shown in **Figure 11** at points 8 and 9.

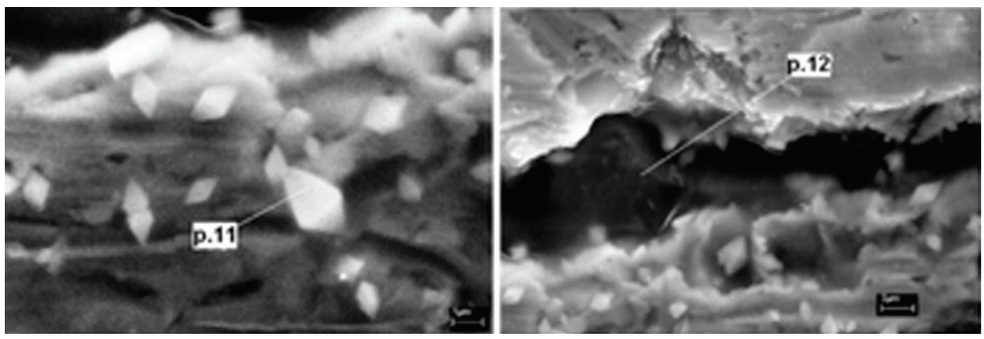

Figure 12. SEM images of the crack and small crystals on the side surface of the palladium wire.

Element	Point 11	Point 12
	at.%	at.%
O	72.1	55.1
Na	1.0	-
Al	0.6	0.7
Si	-	26.9
S	0.2	1.0
Cl	0.1	0.9
K	5.8	1.3
Ca	-	1.8
Mn	0.6	0.8
Fe	0.8	2.3
Ni	-	0.3
Zn	-	0.3
Pd	12.2	8.4
Re	6.6	-
Pt	-	0.2

Table 3. Elements and it concentration crystal deposed in crack vicinity on side surface of palladium specimen (see **Figure 12**).

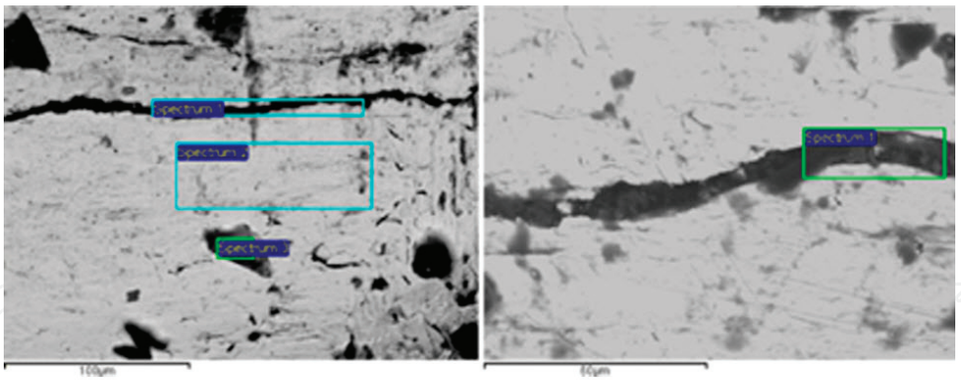

Figure 13. The surface structure of a Re-rod with marked patches for XMA analysis.

Element	C	O	Mg	S	K
Initial	—	—		—	—
Point 1	65.65	17.44		—	—
Point 2	80.94	13.35		0.25	0.10
Point 3	72.95	14.37		—	—
Point 4	72.22	18.90	0.87	0.39	—
Element	Ca	Fe	Re	Os	
Initial	—	—	100	—	
Point 1	—	—	16.07	0.84	
Point 2	—	0.16	4.92	0.28	
Point 3	—	—	11.91	0.77	
Point 4	1.15	—	6.48	—	

Table 4. Elements and it concentration in Re specimen in places shown in **Figure 13**.

carbon layer, with the carbon concentration reaching 80.94 at.%, a rhenium concentration of only 4.92 at.% and relatively high concentration of osmium up to 0.84 at.%.

5. Induced effects in pure gases

Because of some doubts concerning to our results with deuterium-Me systems, by some typical nuclear physicists, analogous investigations aimed at studying the possibilities of nuclear reactions were carried out using hydrogen high pressure chambers (HHPC) in presence of palladium [6] and tin rods, as well as with hydrogen only without any metallic samples inside [15], under irradiation with 10 MeV braking γ-rays. The phenomenological-model approaches for the description of the obtained experimental data on the basis of nuclear fission reactions

http://dx.doi.org/10.5772/intechopen.78740

within the liquid-drop nuclear model and nuclear fission and fusion reactions are presented in Refs. [18, 19].

The goal of this part of chapter is to present results on the synthesis of chemical elements under irradiation of dense molecular H_2, D_2 and atomic He gases, in the absence of metallic samples, with γ-rays of energies near 10 MeV, which has led to the formation of considerably large particles due to physical chemical reactions.

5.1. Results of γ-ray irradiation of the HHPC filled with molecular hydrogen under 1 kbar pressure

Such pressure corresponds to the atomic concentration of hydrogen $n_D \approx 2952 \times 10^{22}$ at.H·cm^{-3} at its density $p_D \approx 0.0494$ g · cm^{-3} (see monograph [20]). Only a manganin foil was placed in the HHPC chamber, and there was no Pd-rod inside. The chamber irradiation was carried out during 14 h (5.04×10^4 s). The electron beam energy was equal to 9.7 MeV at the average current (20–21)μA. During opening of the HHPC, it spilled out eight small particles about 1 mm in size. Some of them were dark, and the other was of light color. When being photographed with a special tool, all of the particles turned out to be transparent.

The photos in **Figure 14** obtained using a special photomicrography tool show the "light" (a) and "dark" (b) particles at about the same scale.

Figure 15 shows SEM images of a dark particle with a size about 703 μm to 628 μm (a) and of its lengthy "tail" (b). Afterwards, this tail was broken during the studies. In regions 17 (a) and 18 (b) from **Figure 15a** and **b**, X-ray microprobe spectrometer (XRMPS) was used.

Table 5 provides the element compositions measured in regions 17 (**Figure 15a**) and 18 for a dark particle from **Figure 15b**. Note that both parts of the dark particle contain only light elements, such as $_6$C, $_7$N↑, $_8$O, $_9$F↑, $_{10}$Ne↑, $_{11}$Na, $_{12}$Mg, $_{13}$Al, $_{14}$Si, $_{15}$P, $_{16}$S, $_{17}$Cl, $_{18}$Ar↑, $_{19}$K, $_{20}$Ca, and a heavier metal $_{29}$Cu. Here is a series of elements with a nucleus charge change by ΔZ = 1 from Z = 6 (carbon) to Z = 20 (calcium), where the volatile elements $_7$N↑, $_9$F↑, $_{10}$Ne↑, $_{18}$Ar↑, which could not have formed any chemical compounds, were not detected. The same refers to the elements which are lighter than carbon and have a nucleus charge Z < 6, i.e., such elements as $_1$D, $_2$He, $_3$Li, $_4$Be and $_5$B, since they cannot be registered by an X-ray microprobe spectrometer.

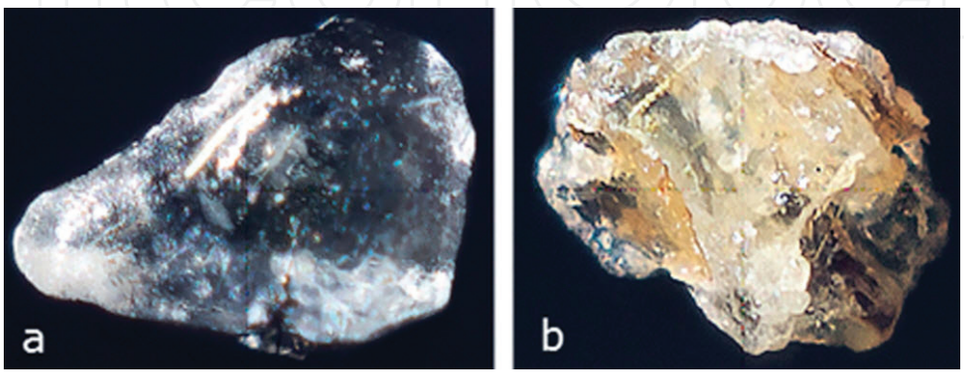

Figure 14. Photos of the "light" (a) and "dark" (b) particles obtained in H_2 gas experiment.

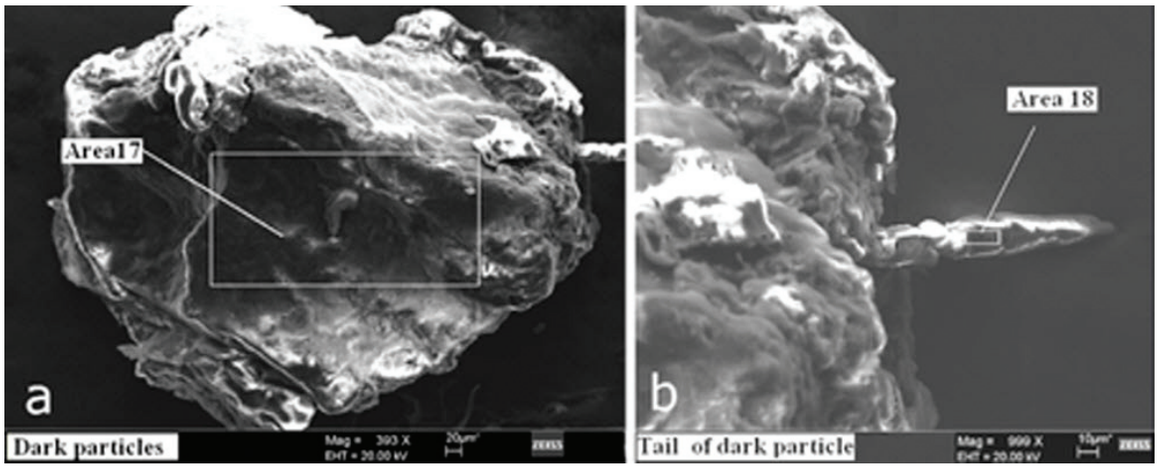

Figure 15. SEM images with a general view of a dark micro particle (a) and its right part with a "tail" (b).

	Figure 15a		Figure 15b		Figure 16a		Figure 18b		Figure 19a		Figure 19b		Figure 21, p. 3		Figure 21b	
El.	**wt.%**	**at.%**	**wt.%**	**at.%**	**wt.%**	**at.%**	**wt.%**	**at.%**	**wt.%**	**at.%**	**wt.%**	**at.%**	**wt.%**	**at.%**	**wt.%**	**at.%**
C	13.0	17.40	25	32.02	47	64.48	43.3	69.30	11.2	17.15	47	66.95	34.2	46.54	25.6	42.44
N													8.1	9.45	5.16	7.34
O	76.7	77.35	68	65.09	26.6	27.31	12.9	15.47	58	66.42	23.1	24.66	37	38.13	26.1	32.65
F							—	—					—	—	—	—
Na	2.49	1.75	1.05	0.70	—	—	—	—	0.62	0.49	—	—	0.23	0.16	—	—
Mg	—	—	0.03	0.02	1.76	1.19	—	—	6.21	4.68	—	—	0.06	0.04	0.51	0.25
Al	0.19	0.11	0.17	0.10	0.24	0.15	0.03	0.02	0.27	0.18	0.11	0.07	0.07	0.04	2.87	2.25
Si	0.22	0.13	0.11	0.06	1.42	0.83	1.03	0.71	1.27	0.83	0.05	0.03	0.10	0.06	—	—
P	0.16	0.08	0.06	0.03	—	—	0.39	0.24	0.02	0.01	0.04	0.02	0.23	0.12	0.30	0.20
S	—	—	0.03	0.02	0.14	0.07	—	—	0.16	0.09	0.12	0.06	0.28	0.14	0.48	0.30
Cl	4.12	1.88	0.45	0.20	0.18	0.08	—	—	0.50	0.26	0 .07	0.03	0.91	0.42	0.89	0.50
K	1.88	0.78	1.37	0.54	0.23	0.09	—	—	0.37	0.17	—	—	0.80	0.33	0.89	0.46
Ca	1.29	0.52	2.18	0.84	0.21	0.09	1.44	0.69	21.0	9.60	1.91	0.82	0.17	0.07	0.87	0.43
Cr	—	—	—	—	—	—	0.31	0.12	—	—	—	—	—	—	—	—
Mn	—	—	—	—	—	—	0.35	0.12	—	—	—	—	—	—	—	—
Fe	—	—	—	—	—	—	35.7	12.32	0.32	0.11	0.40	0.12	0.14	0.04	7.51	2.68
Cu	—	—	1.68	0.41	22.1	5.72	2.37	0.72	—	—	17.0	4.56	17.3	4.44	25.0	7.83
Zn	—	—	—	—	—	—	—	—	—	—	10.24	2.68	—	—	—	—
Sn	—	—	—	—	—	—	1.20	0.19	—	—	—	—	—	—	—	—
Pb	—	—	—	—	—	—	1.03	0.10	—	—	—	—	—	—	—	—

Table 5. The element compositions measured for the marked areas in **Figures 15**, **16**, **18**–**20**.

http://dx.doi.org/10.5772/intechopen.78740

5.2. Results of synthesis of new particles and structures in dense deuterium using the DHPC under the action of γ-rays with 10 MeV energy

Shown in **Figure 3a** modified high-pressure chamber was used for the deuterium experiment with the initial pressure 2.2 kbar with a relative deuterium purity $\approx 10^{-6}$ (see Ref. [4]). The experiment was repeated under a pressure of 3.05 kbar with element 8 made of beryllium bronze.

The modification of the DHPC consisted in the replacement of the viton sealing with the metal-to metal one (beryllium bronze ($CuBe_2$)). This allowed to limit the chemical elements inside the high-pressure chambers filled with gases H_2, D_2 and He (HHPC, DHPC and HeHPC) only to Cu and Be. The initial pressure was constant before irradiation during 2 weeks. The atomic density $n_{D_2} \approx 2.1 \times 10^{22}$ mol.D $\cdot$ cm^{-3} and the mass density $p_{D_2} \approx 0.13$ g $\cdot$ cm^{-3} [20]. The integrated electron fluence at the target was $\approx 2.5 \times 10^{19}$ e$^-$ during the whole experiment. After the irradiation procedure the pressure in the chamber remained constant during 1 month, so leakage of gas was not observed.

The irradiation time was t = 1.76×10^5 s at the electron current 20–21μA. During the irradiation at the stationary state, due to growing temperature an increase of deuterium pressure in the chamber was noted, from initial pressure $p_o \approx 2.085$ kbar at $T_0 = 293$K to $p_{stat} \approx 2.697$ kbar at $T_{stat.} = 343$ K, which means "by jump": $\Delta p \approx 612$ bar. Here, the temperature T_{stat} was measured at the surface of the pressure chamber made of beryllium bronze (**Figure 3**, position 6) inside the protecting sleeve (**Figure 3**, position 11) made from stainless steel.

Taking into consideration the known ideal gases rule [20], the calculated pressure should be: $p_{calc} = 2.441$ kbar.

Thus, the pressure change ought to be $\Delta p_{cal} = p_{calc} - p_o = 356$ bar, as opposed to direct measurement yielding the value $\Delta p_{meas} = 612$ bar. In this situation we can suppose that the temperature inside the beryllium bronze chamber was higher, attaining the value: $T_{stat,cal} = T_0\, p_{stat}/p_o \approx 379$K. That means it was 36 K higher. The interpretation of this difference can be based on the supposition that some nuclear reactions took place during our experiment, It should be noted that in the case of the experiment with hydrogen the calculated growth of pressure during the irradiation was in proper relation to the temperature measured at the surface of the pressure chamber made of beryllium bronze (**Figure 3**, position 6).

5.3. Results of measurements

An accurate SEM and XRMPA observation of the inner surface of the high-pressure chamber and inner surface of the split sleeve and closing element revealed 26 different objects which are described in a preprint published by the Joint Institute of Nuclear Research. Here we will describe only the most interesting and representative results which can be interpreted.

The object found on the inner surface of the window plug (**Figure 3**, p. 4).

Eight interesting objects were found and only two are presented in **Figure 16**. **Figure 16a** shows a curious multiple objects in the form of small pillars, which element composition is given in **Table 5**.

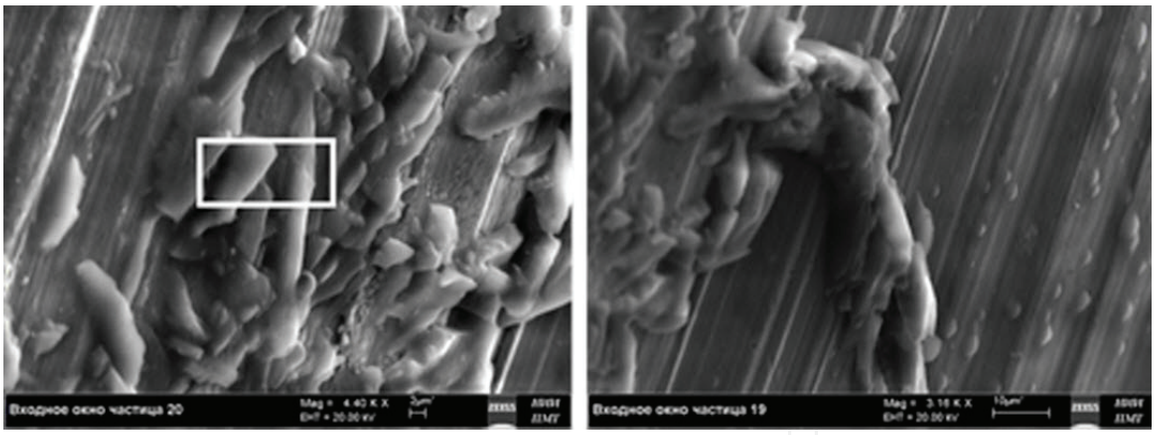

Figure 16. SEM image of the objects found on the window-plug in D_2 experiment.

5.3.1. The object found on the inside surface of the split sleeve: a container for expected products of nuclear reactions

Figure 17 gives a view of the inner surfaces of the first and second halves of the sleeve. We can see dark places on the light surfaces. The element compositions at these places are presented in **Table 6**. In the second case, we can observe a small amount of Cu, which can be interpreted as a large thickness of this object. MPRA used in our experiments collects information from the depth no greater than 4 μm.

5.3.2. The effects observed on the surface of the closing disk made of pure copper

Shown in **Figure 18a** is an image of the closing disc. One can see here similar dark stains as on the surface of the sleeve half (a). **Figure 18b** is a triangular structure on the surface of this disk with a large amount of iron (see **Table 5**).

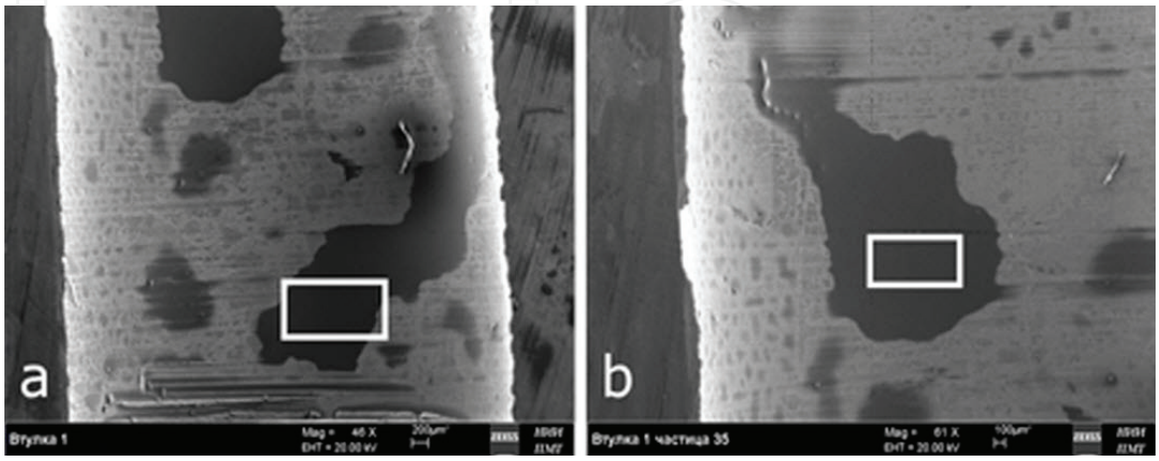

Figure 17. The observed dark stains on the inner surface of the $CuBe_2$ half sleeve, (a) and (b) in the D_2 irradiation experiment.

Element	Z	wt.%	at.%	wt.%	at.%
Area		A		B	
C	6	24.9 ± 3.9	54.92	57 ± 12	65.94
O	8	11.1 ± 1.8	18.36	39 ± 11	33.20
Si	14	0.18 ± 0.04	0.17	—	—
Cu	29	63.8 ± 1.8	26.54	3.97 ± 0.45	0.86

Table 6. The element compositions at the dark spots on the $CuBe_2$ sleeve surfaces, (a) and (b), in the marked areas from **Figure 17**.

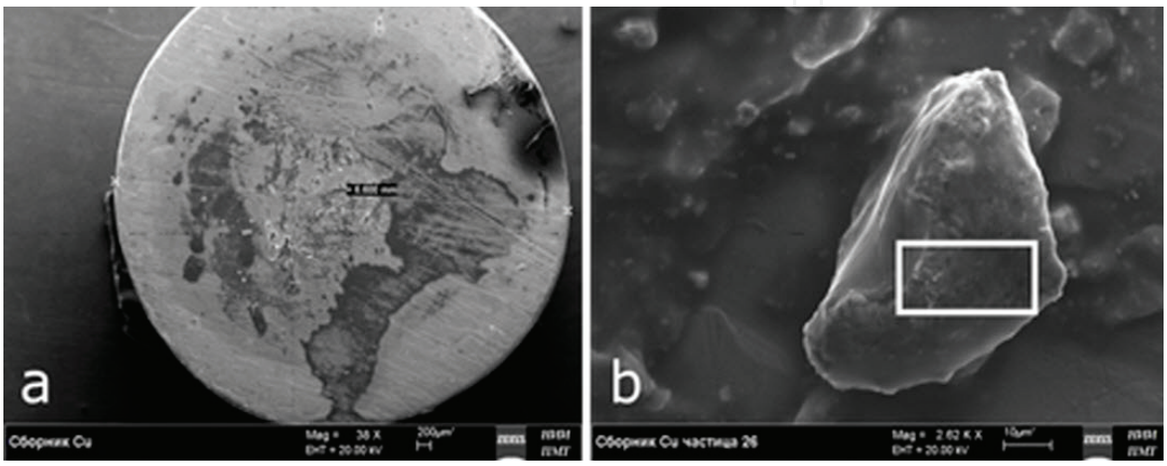

Figure 18. The view of the surface of the closing disk (a) and the found structure (b).

5.3.3. The synthesized structures found during demounting of the pressure chamber, from the left and right parts of the pressure chamber

As mentioned above, many different large particles were found after the irradiation. Here we are going to present only two typical ones. One particle, with a large amount of oxygen and of a rather regular shape, is shown in **Figure 19a**, and its element composition is given in **Table 5**. Another particle, with a large amount of carbon and of a rather non-regular shape, is shown in **Figure 19b**; and its element component is given in **Table 5**, too.

Optical Studies of the Black Oily Foils Synthesized in HeHPC under the Action of Braking γ-rays at Pressure 1.1 kbar.

Upon opening of the chamber, black foils with reinforcing needles were observed at the junction of the entrance window and reaction chamber (see **Figure 3**, pos. 5). Part of the needles protruded from the foils as lengthy white rods of uniform thickness. The foils were then placed on a clean sheet of (tracing) paper. In the place where the black foils were found, the tracing paper was soaked with exudation from the foils. Such exudation resembled synthetic oil or liquid hydrocarbons. In **Figure 20**, the photos obtained using a special device for photomicrography show an array of round black foils which acquired this shape due to the cylindrical symmetry of the reaction chamber's entrance window.

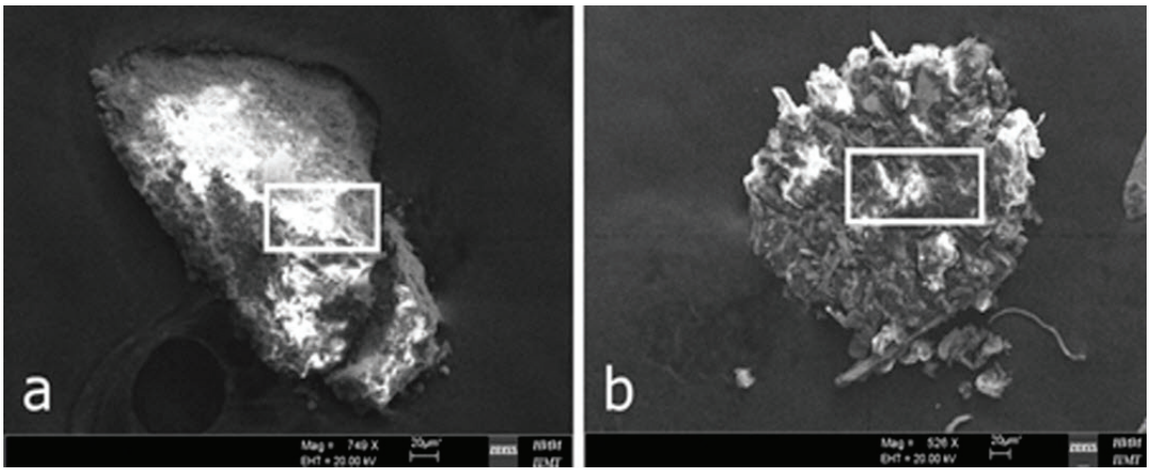

Figure 19. SEM images of the large and regular-shape particles with large amounts of oxygen (a) and with a small amount of oxygen (b) obtained in the D_2 experiment.

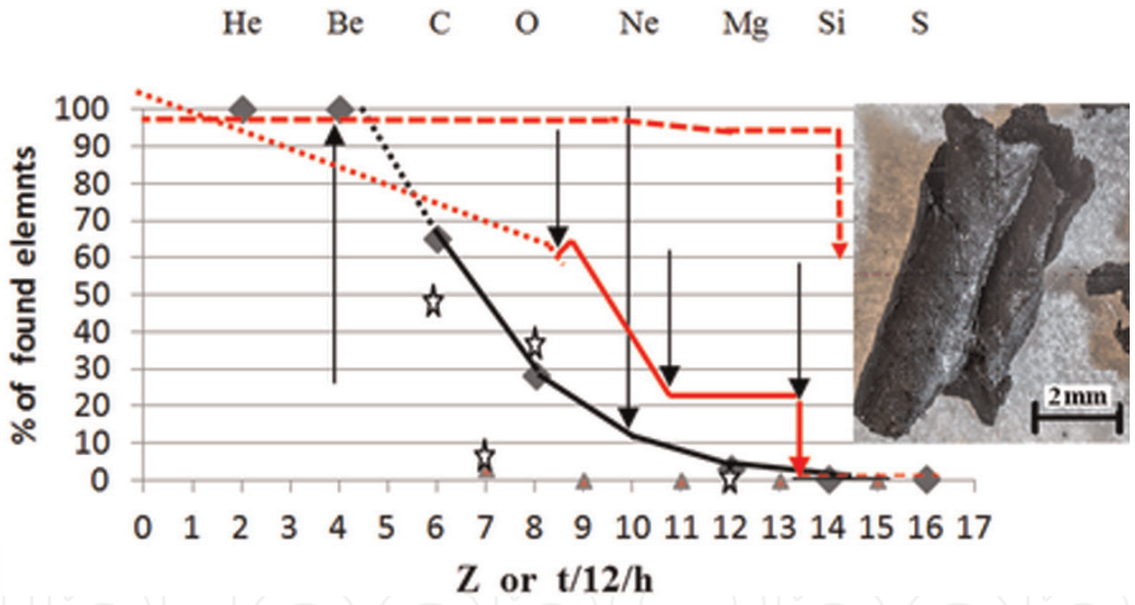

Figure 20. Illustration of the performed experiments with helium carried out using almost the same gamma irradiation procedure. Squares and the red line present first experiment data (p = 1.1 kb); stars and the dotted line correspond to the second experiment (p = 3 kb). On the right the largest object obtained in the first experiment, shown as an example.

Paper [18] (**Figures 2** and **6**) describes other black particles of complex shape obtained in the first experiment. Using the element compositions measured at some points, it was possible to determine some regularities with the help of their mean values (see **Figure 20**).

In a second helium experiment we observed another kind of inhomogeneities. Namely, the main products of synthesis of similar chemical content that covered the surface of the split sleeve surface which is presented in **Figure 21**. This experiment is described in paper [13], here only some, most interesting and representative facts are considered.

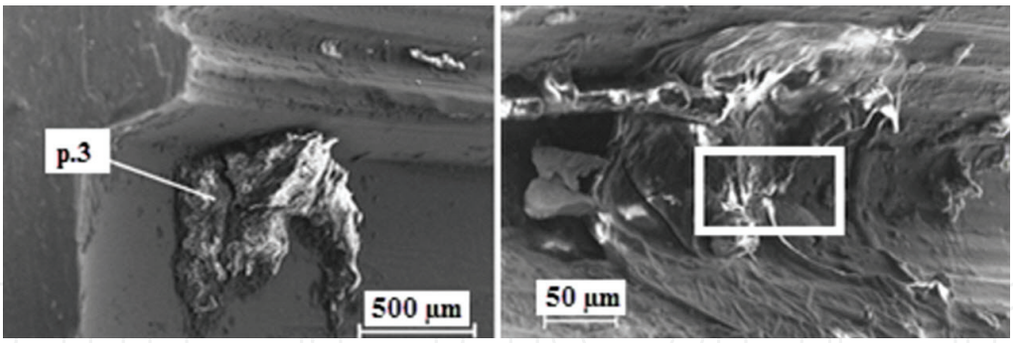

Figure 21. Large particles found near the screw surface obtained in the He experiment.

*5.3.4. The objects found on the inner surfaces of the $CuBe_2$ window-plug (**Figure 3**, position 4)*

At the surface we have observed three interesting objects, one of them being of pyramidal form. These objects are composed mainly of carbon (26.5 at.%), oxygen (62.31 at.%) and potassium (8.33 at.%).

5.3.5. The objects observed on the $Cu_{0.98}Be_{0.02}$ cylinder

On the surface of the cylinder (divided into two equal parts) we could observe 27 different objects. Three of them, of large dimensions and complicated form, located on the wall, are presented in **Figure 21** and their element compositions, in p. 3 and rectangular, are given in **Table 5**.

An example of deposition on a wall and an object of complicated form are shown in **Figure 22**. In the middle, there is a photo of the respective surface before irradiation.

Figure 20 summarizes the element compositions measured for different objects. The curves are given for two experiments with account of the mean values for the element compositions obtained using the MPRA method. Presented curves are different but have a similar character, i.e., a regular decreasing tendency of atomic concentration with a rising atomic number. In

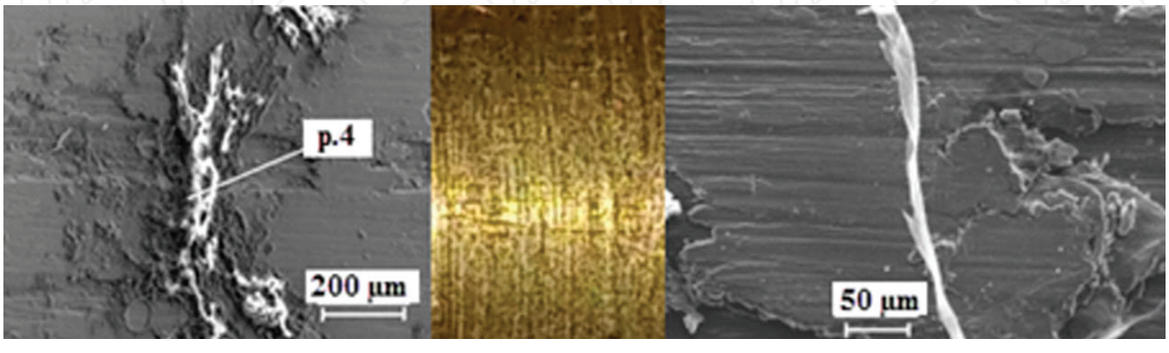

Figure 22. SEM images of the inside surface of the $CuBe_2$ sleeve. Here, we can see specific surface structures and a particle of complex shape. The chemical composition of the particle at p. 4 (in at.%) is as follows: C—39.58, N—9.99, O—39.35, Na—0.69, Cl—1.49, Ca—0.32 and Cu—6.69. In the middle, there is a photo of the respective inside surface of the sleeve prior to irradiation in the second He experiment.

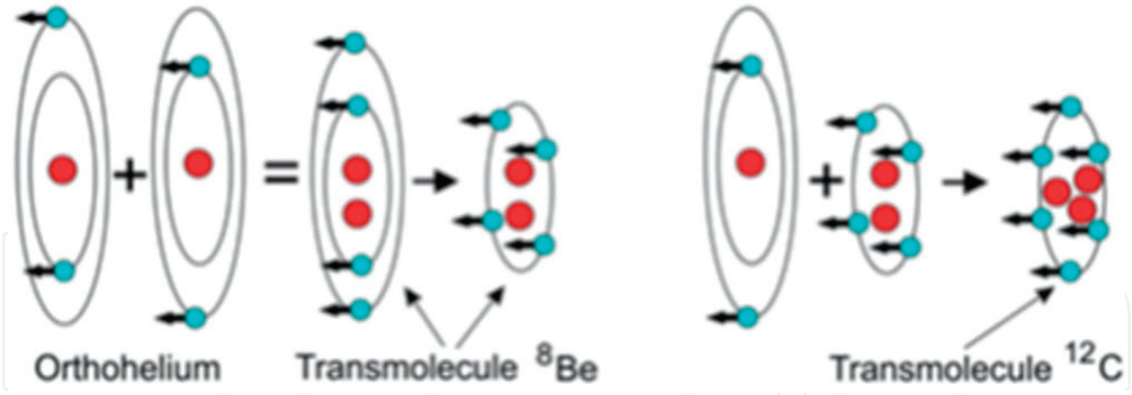

Figure 23. Creation of the stabilized transmolecule of the Carbon $^{12}C_{tr}$. Red point means the α particle [41, 42].

those experiments, inside the HeHPC there was either spectrally pure helium under different pressures or a palladium rod in such helium atmosphere.

All of the three synthesized particles here are the largest objects shown in **Figures 21** and **22** (see also Refs. [12, 13]), and have dielectric properties. According to the X-ray structural analysis, these articles have amorphous structures with a complex hydrocarbon composition that is absent in the reference library of the X-ray analysis. Due to its importance and for the purpose of greater reliability of the data, the structure of synthesized particles was analyzed using microscopes and X-ray micro-analyzers at two independent analytical centers. The mechanical properties of the large particles were not investigated. But there is a most intriguing problem with the electrical properties of the carbon-based structures which we obtained during all the helium experiments. The latest measurements of object shown in **Figure 22** (right upper corner) [30] have shown a very large electrical resistivity $\rho = 10^5 \mu\Omega m$, relative dielectric constant ε = 3–4, low density d = (1.2 ± 0.2)g/cm^3, appeared large paramagnetic properties, having main chemical content C_{62}, O_{31}, Mn_3 wt.%, structure-open problem. In the compression probe we have noted its micro elastic-brittle state with strength 10 MPa (approximate value) and temperature stability bellow 400°C. To interpret these results, phenomenological model of deuteron photo-disintegration with Oppenheimer's reaction, atomic processes of γ-ray scattering on atoms, formation of a di-nuclear system, quasi-classical approach with a two-hump ion potential, internal conversion in solids using a third charged particle, stabilization of nuclei in respect to the β-decay with occupied electronic shells, interpretation of cluster radioactivity, synthesis of elements in astrophysics and element abundance in the Universe were tested in other publications [21–29]. The induced effect in case of helium, referred to multi nuclear reactions in condensed (under high pressure) helium. This process could be considered as cold transmutation of nuclei of chemical elements phenomena, where the unusual detection of transmolecule 12C could be explained as seen in **Figure 23** [30].

6. Conclusions

Induced effects of gamma irradiation at different energies (10 and 23 MeV) were presented in different pure elements and in more complicated systems in details, the results indicated

http://dx.doi.org/10.5772/intechopen.78740

"upstream" nuclear reactions with synthesis of heavier elements and "downstream" reactions with asymmetric fission, with the formation of both light elements from carbon to iron and heavier elements (Ag, Zr, Ba, Ta, W, Pb, Pt, Au) were formed. To interpret these results several models were used. From the authors' point of view, to achieve an accurate description of these effects it is important to elaborate on new approaches to fission and fusion nuclear reactions. Because of volume limit of the chapter, problems including how to explain "protuberation," macro mass changes, so called "Dubna Oscillation," [31] how to realize third step of Tsar bomb (using it for public welfare) author decided to publish it later.

Acknowledgements

Many thanks to Teresa Wilczyńska-Kitowska for her close, long time and fruitful cooperation.

All experiments were carried out according to International (PL-RF) Scientific Cooperation in very efficient, friendly atmosphere, during many years of close cooperation between Polish and Russian teams (presented by Author and Alexander Yu. Didyk) and were financed by both sides.

Author details

Roland Wiśniewski[1,2,3]*

*Address all correspondence to: roland.wisniewski@gmail.com

1 Joint Institute for Nuclear Research, Dubna, Russia

2 National Centre of Nuclear Research, Otwock-Świerk, Poland

3 Physics Faculty, Warsaw University of Technology, Warsaw, Poland

References

[1] Yu DA, Wiśniewski R, Wilczyńska T. Joint Protocol JINR-IAE 2009-2011 and JINR-NCNR 2012-2014. Poland: NCNR; Archives. 2013

[2] Baranowski B, Wiśniewski R. Synteza wodorku niklu z metalicznego niklu i gazowego wodoru. Bulletin de l'Academie Polonaise des Sciences, Serie des Sciences Chimiques. 1966;**14**(4):1273-1275

[3] Wiśniewski R. High pressure apparatus for Gaseous Hydrogen (Deuterium) up to 25 kilobar and temperature range −50°C – +100°C. Review of Scientific Instruments. 1970;**41** (3):455-464

[4] Didyk AY, Wiśniewski R. Nuclear reaction, induced by γ quanta, in palladium saturated with deuterium saturated surrounded by dense deuterium gas. Europhysics Letters. 2012; **99**:22001-22006

[5] Didyk AY, Wiśniewski R. Nuclear Reactions in deuterium-saturated palladium under irradiation by 10MeV γ quanta in dense molecular deuterium at 1.2kbar pressure. Europhysics Letters. 2013;**103**:42002-42008

[6] Didyk AY, Wiśniewski R. Synthesis of micro particles in molecular hydrogen at 1 kbar pressure in nuclear reactions induced by braking γ rays of 10MeV threshold energy. The Chemical Composition and Structures at the Inner Surfaces of the Pressure Chamber Components. Preprint P15-2014-2, Dubna: JINR, RF, 2014. pp 41

[7] Didyk AY, Wiśniewski R. Nuclear reactions in palladium saturated with deuterium and rhenium in dense deuterium gas under irradiation by γ quanta of continuous spectrum with boundary 23MeV energy. Preprint R15-2012-63, Dubna: JINR, 2012. pp. 21

[8] Didyk AY, Wiśniewski R. Results of radiation of aluminum and homogeneous alloy YMn2 by 23MeV energy γ quanta in the atmosphere of molecular deuterium at 2kbar pressure. Preprint P15-2013-41, Dubna, JINR, RF, 2013. pp 18

[9] Didyk AY, Wiśniewski R. Changes observed in the surfaces, bulk properties and chemical composition of vanadium and stainless steel specimens irradiated in dense gaseous deuterium by γ quanta of threshold energy 23 MeV. Preprint P15-2012-75, Dubna: JINR, RF, 2012. pp 14

[10] Didyk AY, Wiśniewski R. Results of radiation of complex system –Al-Y-Mn2- Al- Y-Mn2-Cu- SS by 23MeV energy γ quanta in the atmosphere of molecular deuterium at 2kbar pressure. Preprint P15-2013-41, Dubna: JINR, RF, 2013. pp 19

[11] Didyk AY, Wiśniewski R. Results of radiation of complex system Sn- Mo- Fe-Ni-Bi-Ta-Cu by 23MeV energy γ quanta in the atmosphere of molecular deuterium at 2kbar pressure. To be published

[12] Didyk AY, Wiśniewski R, Wilczyńska-Kitowska T. The carbon-based structures synthetized through nuclear reaction in helium at 1.1kbar pressure under irradiation with braking γ rays of 10mev threshold energy. Europhysics Letters. 2015;**109**:22001-22006

[13] Didyk AY, Wiśniewski R. Synthesis of new structures and substances in dense gases H2, D2, and He under irradiation by braking 10MeV γ rays in $Cu_{0.98}$ $Be_{0.02}$ pressure chamber. JPSA. 2016;**6**(4):13-21

[14] Didyk AY, Wiśniewski R, Wilczyńska-Kitowska, T. Some physical properties of graphite-like object obtained by γ quanta irradiation with threshold energy of 10MeV of pure gaseous he under pressure, in CuBe2 apparatus. JPSA. 2016;**6**(6):1-11

[15] Didyk AY, Wiśniewski R. Synthesis of micro particles in molecular hydrogen at 1kbar pressure in nuclear reactions induced by braking γ rays of 10MeV threshold energy. The chemical composition and structures at the inner surfaces of the pressure chamber components. P15-2014 – 2, pp. 40. Particles and Nuclei, Letters. 2015;**12**(7):1298-1317

[16] Didyk AY, Wiśniewski R, Myshinsky GW, Semin WA, Wilczyńska-Kitowska T. Synthesis of solid-state structures and chemical elements under irradiation by bremsstrahlung γ

rays with maximum energy of 10MeV in condensed deuterium at a pressure of 2.2 kbar. Preprint P15-2018- 3. Dubna: JINR, RF, Particles and Nuclei, Letters 2018, in press. 2018. pp 20

[17] Ishkhanov BA, Kapitonov IM. Interaction of electromagnetic interaction with atomic nuclei. MSU. 1979:215

[18] Bethe H, Morisson P. Elementary Nuclear Theory. New York: John Willey & Sons, Inc; 1956. p. 356

[19] Mukhin KN. Experimental nuclear physics. Physics of Atomic Nucleus. Moscow: Energoatomiz-dat. 1983;**1**

[20] Didyk AY, Wiśniewski R. Properties of hydrogen and its isotopes under high pressure and technological applications. Dubna: JINR. 2013. pp. 320. ISBN: 978-5-9530-0358-2

[21] Sierk AJ. Mass-assimetric fission of light nuclei 1985. Macroscopic Model of Rotating Nuclei. Physics Review. 1986:**55**(6):582-583

[22] Oppenheimer JR, Fillips M. Note for the transmission functions for deuteron. Physics Review. 1935;**48**(15):500-502

[23] Tarakanov AV, Shilov VM, Schmidt R. Nuclear Physics. 1991;**53**(5):1285-1291

[24] Shilov VM. Sub-barrier fusion of spherical nuclei of medium atomic number. Nuclear Physics. 2012;**75**(4):485-490

[25] Kálmán P, Keszthelyi T. Lattice effects in solid state internal conversion. Nuclear Physics. C79. 2009;**031602**(R):P.031602-1-031606-4

[26] Bosch F, Faestermann T, Friese J, et al. Observation of bound-state β- decay of fully ionized ^{187}Re: ^{187}Re - ^{187}Os Cosmochronometry Decay. Physical Review Letters. 1996;**77**(26):5190-5193

[27] Volkov V V, Cherepanov EA. Formation of nuclear molecules in cluster radioactivity. On interpretation of the cluster radioactivity mechanism. Physics of Particles and Nuclei Letters. 2013;**3**(180):347-353

[28] Ishkhanov BS, Kapitonov IM, Tutyn IAM. LIBROKOM. 2009. http://nuclphys.sinp.msu.ru/nuclsynt.html

[29] Bethe HA. Energy production in stars. Physics Review. 1939;**55**:434-456

[30] Mishinsky GV. Multinuclear reaction in condensed helium. Nuclear Physics. 2017;**9**(1):94-105. RENSIT and Nuclear Physics, RENSIT. Atom in a strong magnetic field. Transformation of atoms into transatoms. 2017;**9**(2):147-160

[31] Wiśniewski R, Wilczyńska-Kitowska T, Didyk AY. Dubna oscillations phenomenon. In preparation for publication

IntechOpen